© 2023. Published by The Company of Biologists Ltd | Journal of Cell Science (2023) 136, jcs260598. doi:10.1242/jcs.260598

RESEARCH ARTICLE

The cytoplasmic tail of the mechanosensitive channel Pkd2 regulates its internalization and clustering in eisosomes

Mamata Malla, Debatrayee Sinha, Pritha Chowdhury, Benjamin Thomas Bisesi and Qian Chen*

ABSTRACT

Polycystins are a family of conserved ion channels, mutations of which lead to one of the most common human genetic disorders, namely, autosomal dominant polycystic kidney disease. *Schizosacchromyces pombe* possesses an essential polycystin homologue, Pkd2, which directs Ca^{2+} influx on the cell surface in response to membrane tension, but its structure remains unsolved. Here, we analyzed the structure–function relationship of Pkd2 based on its AlphaFold-predicted structure. Pkd2 consists of three domains, the extracellular lipid-binding domain (LBD), nine-helix transmembrane domain (TMD) and C-terminal cytoplasmic domain (CCD). Our genetic and microscopy data revealed that LBD and TMD are essential for targeting Pkd2 to the plasma membrane from the endoplasmic reticulum. In comparison, CCD ensures the polarized distribution of Pkd2 by promoting its internalization and preventing its clustering in the eisosome, a caveolae-like membrane compartment. The domains of Pkd2 and their functions are conserved in other fission yeast species. We conclude that both extracellular and cytoplasmic domains of Pkd2 are crucial for its intracellular trafficking and function. We propose that mechanosensitive channels can be desensitized through either internalization or clustering in low-tension membrane compartments.

KEY WORDS: Polycystin, Pkd2, *Schizosaccharomyces*, Fission yeast, Cytokinesis, Transmembrane, Eisosome, ER–PM contact

INTRODUCTION

Polycystins are a family of transmembrane proteins that are evolutionarily conserved from yeast to humans. Loss-of-function mutations in either one of two human polycystin genes, *PKD1* (encoding PC-1) and *PKD2* (encoding PC-2), results in autosomal dominant polycystic kidney disease (ADPKD). ADPKD is one of the most common human genetic disorders, affecting one in 1000 live births in the world (Burn et al., 1995; Mochizuki et al., 1996). PC-1 is a putative G-protein coupled receptor (GPCR)-like mechanosensor (Geng et al., 1996; Parnell et al., 2018; Su et al., 2015). In comparison, PC-2 oligomerizes into a Ca^{2+}-permissive transient receptor potential (TRP) channel, but it permeates monovalent cations such as K^+ and Na^+ much better than Ca^{2+} (Foggensteiner et al., 2000; Liu et al., 2018; Pazour et al., 2002). Together, these two human polycystins are also capable of assembling into a hetero-tetrameric channel (Grieben et al., 2017; Su et al., 2018). The polycystin channel is presumably activated by fluid flow in kidneys to regulate the Ca^{2+} homeostasis in primary cilia (Nauli et al., 2003). In addition to its function in kidneys, PC-2 also promotes left-right determination during embryonic development of vertebrates (Pennekamp et al., 2002). Overall, polycystins play a wide range of cellular and developmental functions, many of which depend on them being at the right intracellular compartments.

The intracellular trafficking of polycystins is rather complex. PC-1 undergoes proteolysis that cleaves this GPCR-like protein into two: an extracellular fragment including dozens of immunoglobin-like repeats called PKD domains, and another fragment consisting of all the transmembrane helices and the cytoplasmic tail (Qian et al., 2002). These two PC-1 fragments nevertheless interact with each other on the cell surface. In comparison, the other polycystin, PC-2, can be found at both the cell surface and the endoplasmic reticulum (ER) (Cai et al., 1999). On the plasma membrane (PM), this TRP channel is sorted into the primary cilium (Pazour et al., 2002). Adding to the complexity, polycystins also localize to extracellular vesicles (Hogan et al., 2009; Wang et al., 2014). The underlying molecular mechanisms regulating the intracellular trafficking of polycystins remain largely unknown.

Schizosacchromyces pombe (*S. pombe*), commonly known as fission yeast, presents an attractive unicellular model to study the evolutionally conserved polycystin channels. This model organism possesses an essential polycystin homologue, Pkd2. This putative TRP channel (Palmer et al., 2005) is targeted to the PM, but it also localizes to intracellular membrane compartments (Morris et al., 2019). In the PM, the channel stays within the cell tips during interphase growth, before translocating to the equatorial plane during cell division. Pkd2 is an essential protein required for cell proliferation, including both cell division and cell growth (Morris et al., 2019; Sinha et al., 2022). In cytokinesis, the last stage of cell division, Pkd2 modulates contractile ring constriction at the beginning and promotes cell separation at the very end (Morris et al., 2019). This channel also antagonizes the essential yeast Hippo-like signaling pathway septation initiation network (SIN). As a result, mutations of *pkd2* partially rescue the lethal SIN mutation (Sinha et al., 2022). During interphase growth, Pkd2 promotes cell tip extension by regulating turgor pressure. A temperature-sensitive mutation, *pkd2-B42*, leads to significantly reduced cell tip growth and a failure to maintain cell volume homeostasis, a unique phenotype termed ‘deflation’ (Sinha et al., 2022).

As an ion channel, Pkd2 permeates Ca^{2+} when it is activated by mechanical force. *In vitro*-reconstituted Pkd2 can be activated by membrane stretching (Poddar et al., 2022). This mechanosensitivity allows Pkd2 to direct the Ca^{2+} influx during both the osmotic adaption and the separation of daughter cells during cytokinesis (Poddar et al., 2022, 2021). However, it remains unknown how Pkd2 is targeted to the PM, where it can sense membrane tension.

Department of Biological Sciences, The University of Toledo, 2801 West Bancroft Street, Toledo, OH 43606, USA.

*Author for correspondence (qian.chen3@utoledo.edu)

Q.C., 0000-0002-2768-6570

Handling Editor: John Heath
Received 1 September 2022; Accepted 25 May 2023

Journal of Cell Science (2023) 136, jcs260598. doi:10.1242/jcs.260598

In this study, we took advantage of the new AlphaFold (Jumper et al., 2021)-predicted structure of Pkd2 to examine how its three domains, the lipid-binding domain (LBD), the transmembrane domain (TMD) and C-terminal cytoplasmic domain (CCD), contribute to its intracellular localization and function. We constructed a series of Pkd2 truncation mutants, characterized their localization by fluorescence microscopy and tested their function through genetic analyses and quantitative microscopy. We discovered that LBD is essential for the targeting of Pkd2 to the PM. The cytoplasmic tail or CCD plays a crucial role in the intracellular trafficking of Pkd2, including its clustering in eisosomes and selective internalization. This mechanism of trafficking largely determines the polarized localization of Pkd2 on the cell surface. We also compared *S. pombe* Pkd2 to its homologues from another fission yeast *S. japonicus* and humans for their intracellular trafficking as well as function. Overall, our results revealed that targeting of the mechanosensitive Pkd2 to its active sites requires both its cytoplasmic tail and the extracellular domain. We proposed a novel model regulating the intracellular trafficking of this essential ion channel.

RESULTS

AlphaFold-predicted tertiary structure of Pkd2

As the structure of fission yeast Pkd2 has not been experimentally determined, we employed AlphaFold to predict its putative domains and their respective structures. Preliminary analysis of the primary and secondary structures of Pkd2 suggested that it possesses a 23 amino acid (aa) N-terminal signal peptide (SP). It is projected to be cleaved in the ER (probability of 96%), based on the analysis by SignalIP6.0 (Teufel et al., 2022). To test this hypothesis, we tagged the N-terminus of Pkd2 with GFP at the endogenous locus. Consistent with the cleavage of the SP in the ER lumen, the fluorescence of GFP–Pkd2 marked the ER membrane exclusively (Fig. S1A, left). This was in contrast to the C-terminally tagged Pkd2–GFP, which localized to the PM and was largely absent from the ER (Fig. S1A, middle) (Morris et al., 2019). Although the yeast ER network looks similar to the PM in some extents, three features distinguish them from each other. Firstly, only the ER network distributes around the nucleus (Fig. S1A, left). Secondly, only the ER network consists of the unique tether structure linking the cortical and peri-nuclear ER (Fig. S1A, left). Lastly, only the PM is enriched at the equatorial plane of a dividing cell during cleavage furrow ingression, whereas the ER is excluded from the plane (Fig. S1A, left) (Marek et al., 2020; Vještica et al., 2020; Zhang et al., 2012). The intracellular distribution of GFP– Pkd2 fluorescence completely matched that of the ER, represented by the ER marker mCherry–ADEL (Fig. S1D). Another fusion protein, SP–GFP– Pkd2, sandwiching GFP between the SP and the rest of Pkd2, expressed poorly (Fig. S1A, right), but its fluorescence was detectable at the PM as the C-terminally tagged Pkd2–GFP was. Thus, like many other integral membrane proteins, Pkd2 possesses an N-terminal SP removed in the ER during translation.

The SP of Pkd2 is followed by three putative domains: a 147 aa putative LBD, a 405 aa TMD and a 135 aa CCD (Fig. 1A). Largely agreeing with this, AlphaFold predicted a tripartite structure of three distinct domains (Fig. 1B), with high confidence for the LBD and TMD. In this structure, the extracellular N-terminal LBD adopts an immunoglobulin (Ig)-like fold (Bork et al., 1994), consisting of two opposing β-sheets, each with four anti-parallel β-strands (A to H) (Fig. 1C). A hydrophobic cavity is projected to form between the two β-sheets, with potential lipid-binding capacity. Two pairs of cysteine, C36/C155 and C92/C100, likely stabilize the IgG fold (Fig. 1C). Unlike either human PC-1 or PC-2, the TMD of yeast Pkd2 contains nine projected transmembrane helices (Fig. 1D) that make extensive contacts with the LBD. The CCD, the structure of which was predicted with the lowest confidence among the three domains, consists of mostly disordered sequences (Fig. 1B). Contrary to the previous secondary structure prediction (Morris et al., 2019), AlphaFold found no coiled-coil motif in the CCD. As human polycystins can form either homo- or hetero-tetramers, we also employed AlphaFold to calculate the structure of the Pkd2 homo-tetramer, but the algorithm failed to make any high-confidence predictions. Based on these computational analyses, we concluded that Pkd2 most likely consists of the three structurally distinct domains, i.e. LBD, TMD and CCD.

Both the LBD and TMD of Pkd2 are required for its localization and function

Based on the structural prediction, we expressed each of the three Pkd2 domains separately to determine their localization and function. They were tagged with GFP, expressed from an exogenous locus driven by the strong actin promoter in wild-type yeast cells, except for LBD, the expression of which was driven by the *3nmt1* promoter. Both LBD–GFP and CCD–GFP diffused throughout the cytoplasm (Fig. S1B,C). In comparison, TMD–GFP stayed in the ER, marked by mCherry–ADEL, instead of localizing to the PM as the full-length protein does (Fig. S1D). Not surprisingly, this ER-localized TMD failed to rescue the deletion mutant *pkd2Δ* (Fig. S1E). Therefore, none of the three domains are targeted to the PM on their own.

Next, we determined which of these three domains was indispensable for the function of Pkd2. As *pkd2* is an essential gene (Morris et al., 2019), we tested this by replacing the full-length gene with three truncation mutants: *pkd2ΔLBD*, *pkd2ΔTMDΔCCD* or *pkd2ΔCCD*, expressed at the endogenous locus. The first two were inviable (Fig. 1E,F). In contrast, the last one without CCD was viable, achieving similar growth as the wild type did at temperatures ranging from 25 to 36°C (Fig. 1G). We concluded that both the LBD and TMD domains are essential for the function of Pkd2 but CCD is not.

Curiously, the TMD of Pkd2 is projected to possess more transmembrane helices than human polycystin PC-2 (six helices), but less than PC-1 (11 helices). To determine whether all the transmembrane helices of Pkd2 are essential, we systematically removed one or more of them from Pkd2 to generate a series of overexpressed truncation mutants (Table S1). However, all these Pkd2 mutants were retained in the ER, unable to reach the PM (Table S1). None of them rescued the temperature-sensitive mutant *pkd2-B42* (Sinha et al., 2022) (Table S1), unlike the full-length protein, which even fully rescued the *pkd2Δ* mutant (Fig. S2A–C). Thus, all nine transmembrane helices are essential for the intracellular trafficking of Pkd2.

CCD-less Pkd2 becomes depolarized in the PM and clustered in eisosomes

To determine the potential function of CCD, we first characterized how it regulates the intracellular trafficking of Pkd2. We compared the localization of Pkd2–GFP and Pkd2ΔCCD–GFP, both driven by the native promoter and expressed from the endogenous locus (Fig. 2A,B). Consistent with our previous study (Morris et al., 2019), we found that full-length Pkd2 was targeted to the PM of cell growth sites, including both the cell tips and equatorial division plane (Fig. 2B). In comparison, the distribution of Pkd2 on the cell surface was polarized, enriched at the tips, whereas the distribution

Journal of Cell Science (2023) 136, jcs260598. doi:10.1242/jcs.260598

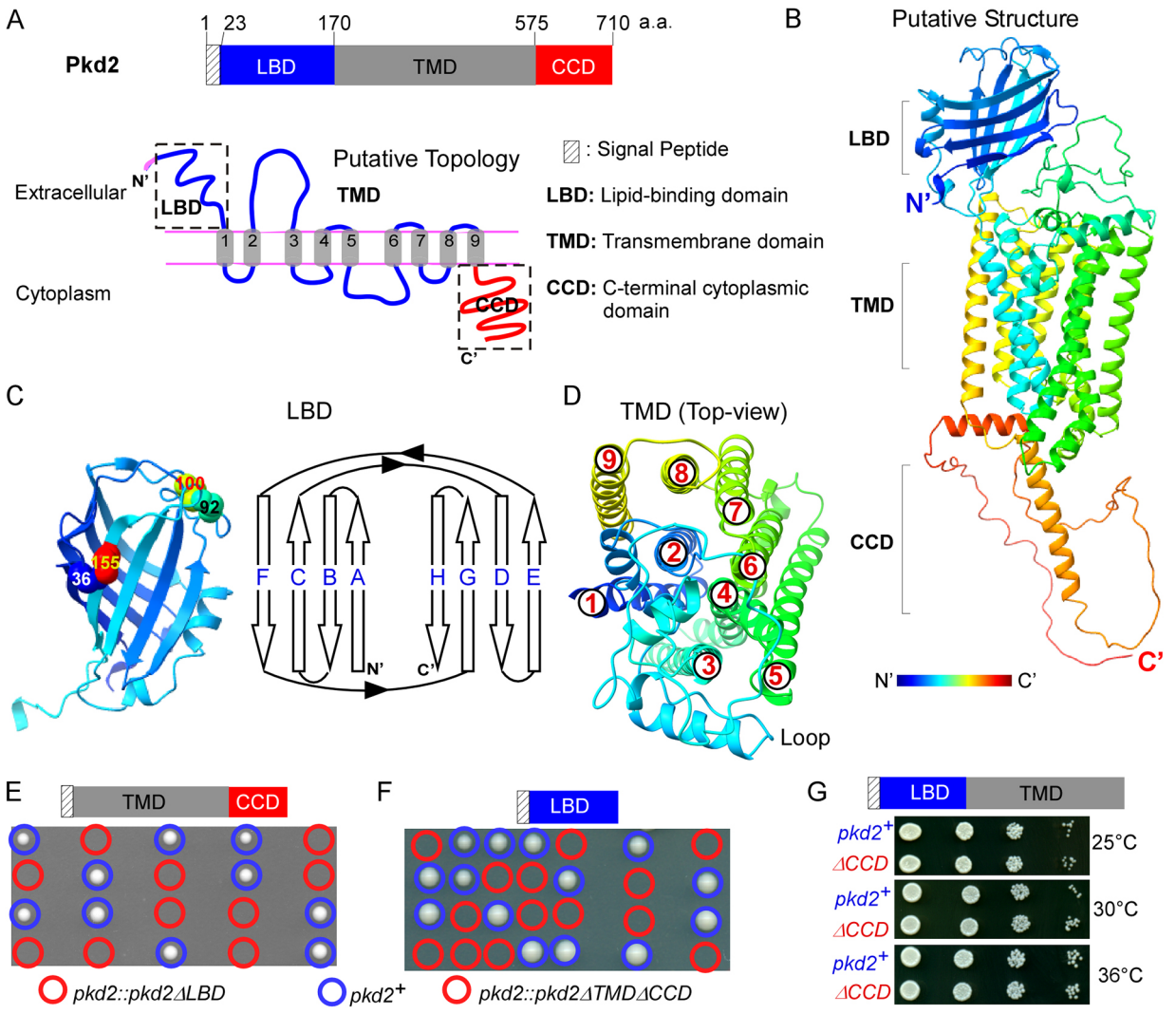

Fig. 1. AlphaFold-predicted structure of Pkd2. (A) Schematics of the primary structure (top) and topology (bottom) of Pkd2. The topology was predicted using Protter (Omasits et al., 2014). (B) Ribbon diagram of the AlphaFold-predicted tertiary structure (rainbow colored) of Pkd2. The signal peptide (SP) is projected with high confidence to be cleaved (SignalIP6.0; Teufel et al., 2022); therefore, it was not included. The structure was rendered using ChimeraX. (C,D) Ribbon diagrams of the structures of LBD (C) and TMD (D). (C) Left: side-view of LBD with two pairs of cysteines labelled and rendered with surface view. Right: 2D topology of eight β-strands (labeled A to H) in LBD. (D) Top view of the nine transmembrane helices (labeled 1 to 9) in TMD. (E,F) Representative tetrad dissection plates of sporulated diploids *pkd2*$^{+}$/*pkd2ΔLBD* (E) and *pkd2*$^{+}$/*pkd2ΔTMDΔCCD* (F). At least 20 tetrads were dissected for each. Neither *pkd2::pkd2ΔLBD* (red circles) nor *pkd2::pkd2ΔTMDΔCCD* (red circles) was viable. (G) Ten-fold dilution series of yeast on YE5S plates at various temperatures. *pkd2::pkd2ΔCCD* grew similarly as the wild type. Images are representative of three independent experiments.

of the truncation mutant was not (Fig. 2C). In addition, the full-length Pkd2 was also found in many intracellular membrane compartments of various sizes (Fig. 2B,D). The smaller compartments were often marked by the endosomal marker Cfr1 (Hoya et al., 2017) (Fig. 2B). The larger ones were usually in the lumen of vacuoles, the yeast equivalent of lysosomes, identified by the integral vacuolar membrane protein Vph1 (Mulholland et al., 1999) (Fig. 2D). In contrast, although Pkd2ΔCCD–GFP continued to be targeted to the PM, it was not restricted to the growth sites of cell tips anymore (Fig. 2B–D). The truncated Pkd2 was mostly absent from either Cfr1-labeled endosomes or Vph1-labeled vacuoles (Fig. 2B,D). Therefore, CCD promotes both the polarized distribution of Pkd2 in the PM and the sorting of Pkd2 through the endocytic pathway to vacuoles.

Next, we focused on how CCD regulates the distribution of Pkd2 in the PM by imaging the cell surface through confocal microscopy (Fig. 3A). Unlike the full-length protein, which concentrated towards the cell tips and the division plane on the cell surface, Pkd2ΔCCD–GFP clustered in a network of intertwined short filaments. Its appearance was similar to that of eisosomes, which are caveolae-like invaginating microdomains of the yeast PM (Fig. 3A) (Kabeche et al., 2011). Indeed, these Pkd2ΔCCD–GFP filaments partially overlapped with eisosomal filaments, marked by Pil1–mCherry, with the average Pearson's colocalization coefficient of ∼0.3 (Fig. 3A,B). In contrast, the colocalization between the full-length Pkd2 and Pil1 was close to zero (Fig. 3A,B). Without eisosomes, Pkd2ΔCCD failed to form any clusters in the *pil1*-deleted cells (Fig. S3A) (Kabeche et al., 2011). We concluded that CCD-less Pkd2 is targeted to the eisosomes in the PM where this channel clusters into short filaments (Fig. 3A,C).

As eisosomes associate closely with the contact sites between ER and the PM (Ng et al., 2020), we asked whether these membrane contacts regulate the clustering of Pkd2ΔCCD as well. We determined the localization of Pkd2ΔCCD–GFP in the mutants of

Journal of Cell Science (2023) 136, jcs260598. doi:10.1242/jcs.260598

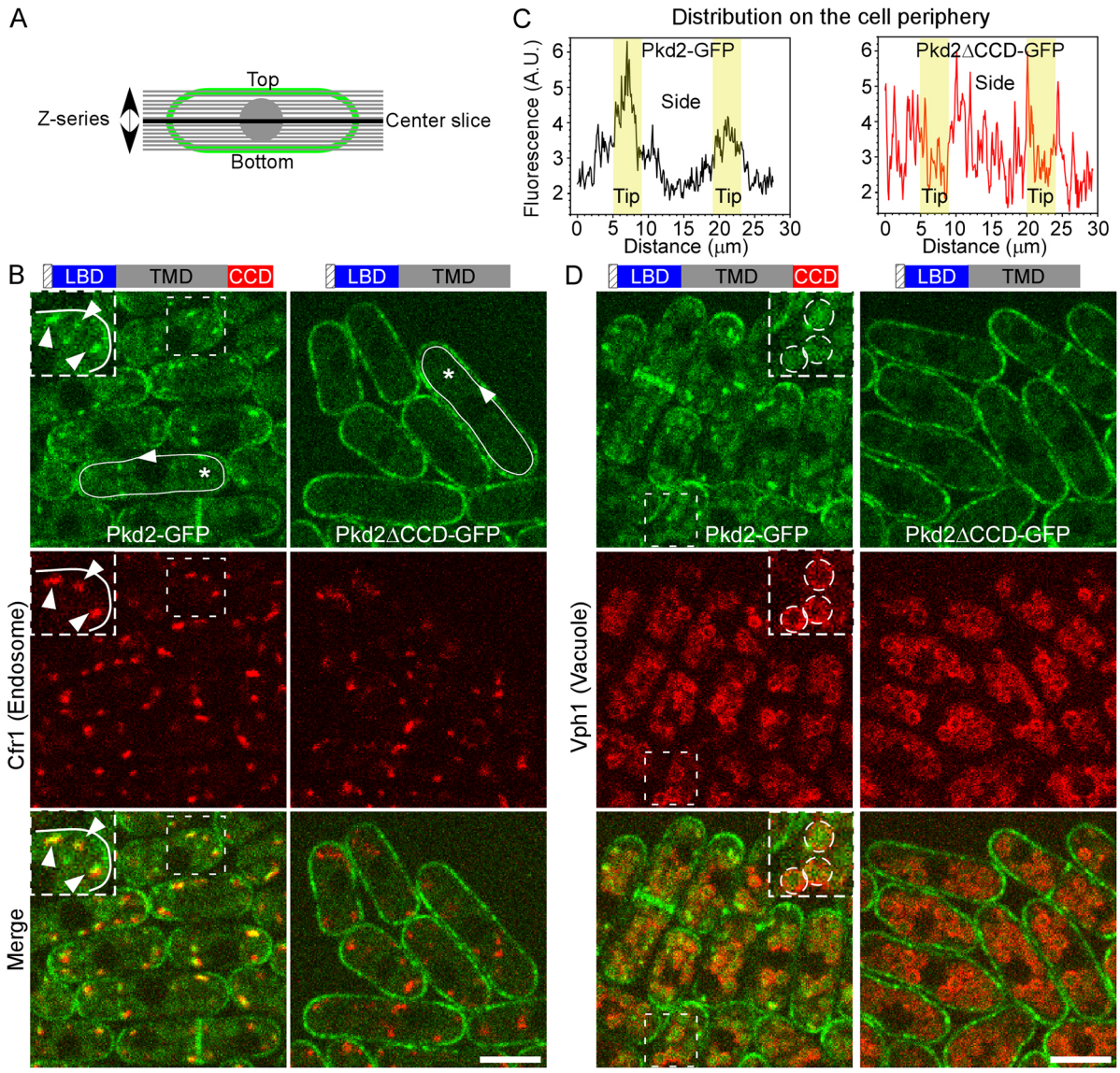

Fig. 2. CCD promotes the intracellular trafficking of Pkd2 to endosomes and vacuoles. (A) Diagram of the center slice in the confocal *z*-series of a cell (side view). (B,D) Micrographs (center slice) of the cells co-expressing either Pkd2–GFP (green, top) or Pkd2ΔCCD–GFP (green, top) and either the endosomal marker Cfr1–mCherry (red, middle, B) or the vacuole marker Vph1–mCherry (red, middle, D). The merged micrographs are shown at the bottom. Dashed boxes are magnified views of representative cells. Arrowheads indicate endosomes where Pkd2 and Cfr1 colocalized. Circles indicate vacuoles, outlined by Vph1, with Pkd2 in the lumen. In contrast to the full-length protein, Pkd2ΔCCD–GFP was largely absent from either eisosomes or vacuoles. Images are representative of three independent experiments. Scale bars: 5 µm. (C) Line scans of the periphery of two representative cells (asterisks in B) expressing either Pkd2–GFP or Pkd2ΔCCD–GFP. Although the full-length protein was concentrated at the cell tips (shaded area), the truncation mutant was not. A.U., arbitrary units.

scs2 and *scs22*, encoding two VAMP-associated proteins, which are tethers between the ER and PM (Manford et al., 2012; Zhang et al., 2012). As reported previously (Ng et al., 2020), deletion of *scc2* and *scs22* reduced the number of the eisosomal filaments in *scs2Δscs22Δ* cells but increased the filament length compared to those of wild-type cells (Fig. 3A). In correlation, Pkd2ΔCCD filaments in these *scs2Δscs22Δ* cells also became longer and more distinct than those of wild-type cells. Pearson's colocalization coefficient between Pkd2ΔCCD and Pil1 doubled to 0.6 in *scs2Δscs22Δ* cells compared to that in the wild type (Fig. 3B). In comparison, full-length Pkd2 did not cluster visibly in eisosomes in *scs2Δscs22Δ* cells (Fig. S3C). Although there was no genetic interaction between *pkd2ΔCCD* and *pil1Δ* mutants (Fig. S3B), we found a strong negative genetic interaction between the temperature-sensitive mutant *pkd2-B42* and *pil1Δ* (Fig. 3D), consistent with the role of eisosomes in the intracellular trafficking of Pkd2. We concluded that ER–PM contacts modulate the clustering of Pkd2ΔCCD in eisosomes.

Lastly, we examined how the clustering of Pkd2ΔCCD affects its translocation to the equatorial division plane. During cytokinesis, the GFP-tagged full-length protein was targeted to the equatorial division plane, coinciding with the start of the contractile ring constriction (Fig. 4A,B). Pkd2ΔCCD–GFP acted similarly during cytokinesis (Fig. 4B). The fluorescence intensity of Pkd2ΔCCD–GFP at the division plane peaked just as ring constriction completed (Fig. 4C), but the intensity decreased by ∼50% compared to that of the full-length Pkd2–GFP (Fig. 4C), despite their similar expression levels (Fig. S3D). More differences lay in their kinetics. Whereas

Journal of Cell Science (2023) 136, jcs260598. doi:10.1242/jcs.260598

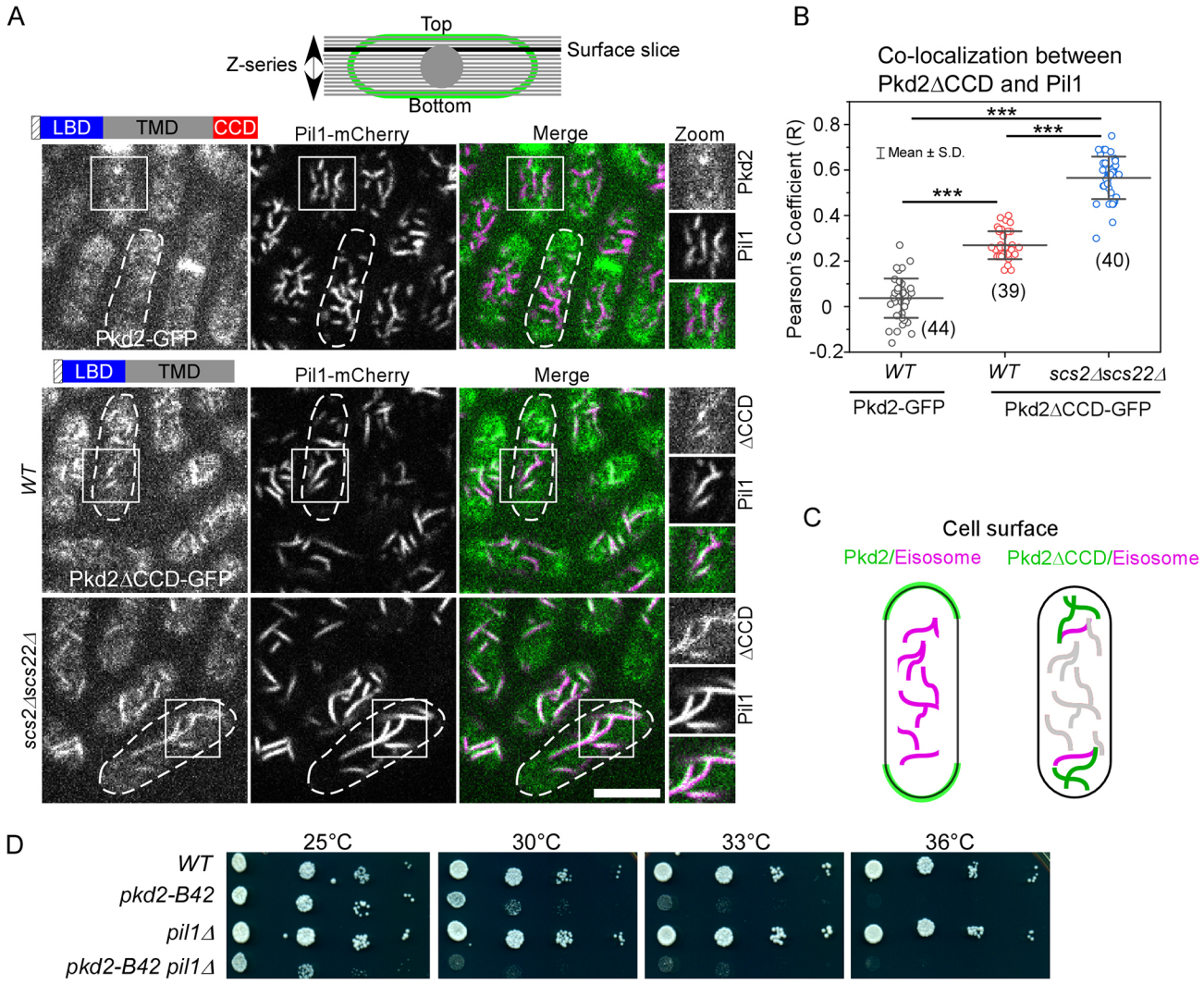

Fig. 3. Pkd2ΔCCD clusters in eisosomes in the plasma membrane. (A) Top: diagram of the surface slice in the confocal *z*-series of a cell (side view). Bottom: micrographs (surface slice) of the cells co-expressing either Pkd2–GFP (top) or Pkd2ΔCCD–GFP (middle and bottom) and the eisosomal marker Pil1–mCherry. The merged micrograph is pseudo-colored with Pkd2 or Pkd2ΔCCD in green and Pil1 in magenta. *WT*: wild-type cells. Dashed lines indicate outlines of the representative cells. Rectangles indicate the selected cell surface area for the zoomed-in view (right). Scale bar: 5 µm. (B) Dot plot of the average Pearson's colocalization coefficient between Pil1–mCherry and either Pkd2–GFP or Pkd2ΔCCD–GFP on the cell surface. ***$P \leq 0.0001$ (one-way ANOVA followed by two-tailed paired Student's *t*-tests). Numbers indicate the total number of cells analyzed. Bars show mean±s.d. Data are from at least two independent biological repeats. (C) Diagrams of the localization of Pkd2 (left) and Pkd2ΔCCD (right) in the plasma membrane (PM), based on A and B. Full-length Pkd2 (green) concentrates at the cell tip region of the PM, largely segregated from eisosomes (magenta). In contrast, CCD-less Pkd2 clusters throughout the cell surface, including at eisosomes, modulated by ER–PM contacts. (D) Ten-fold dilution series of yeast on YE5S plates at various temperatures. The double mutant *pkd2-B42 pil1Δ* grew very poorly even at the permissive temperatures of 25 and 30°C, unlike the temperature-sensitive mutant *pkd2-B42*. Images are representative of two independent experiments.

the fluorescence intensity of Pkd2ΔCCD–GFP remained constant throughout the cell separation, the intensity of the GFP-tagged full-length protein decreased gradually (Fig. 4C). Deletion of *pil1*, which is required for eisosome assembly, slightly increased the localization of Pkd2ΔCCD–GFP at the equatorial division plane by ∼20% (P=0.03) (Fig. S3E). Thus, CCD is necessary for the effective trafficking of Pkd2 to the equatorial plane during cytokinesis.

Although it is clear that CCD regulates the localization of Pkd2, we wondered whether it has a role in the function of this transmembrane protein. As Pkd2 is required for cell tip expansion and cytokinesis, we quantified tip growth and cytokinesis of *pkd2::pkd2ΔCCD* mutant cells through time-lapse microscopy. In comparison to the wild-type cells, *pkd2::pkd2ΔCCD* cells extended their tips only at a slightly higher rate (Fig. 4D). Likewise, both the contractile ring constriction and cell separation proceeded mostly unperturbed in the truncation mutant cells (Fig. 4E,F). We concluded that CCD is largely dispensable for the cellular functions of Pkd2 in cell proliferation, despite its essential role in regulating the intracellular trafficking of Pkd2.

Comparisons among Pkd2 and its two *S. pombe* paralogues

AlphaFold predicted that two other putative ion channels in *S. pombe* share a similar tripartite structure with Pkd2 (Fig. 5A), despite their overall sequence identity being only ∼20%. Like Pkd2, both Trp663 and Trp1322 possess a 23 aa N-terminal SP that is projected to be cleaved at the ER. Consistent with this prediction, in cells expressing the N-terminally tagged GFP–Trp663, the

Journal of Cell Science (2023) 136, jcs260598. doi:10.1242/jcs.260598

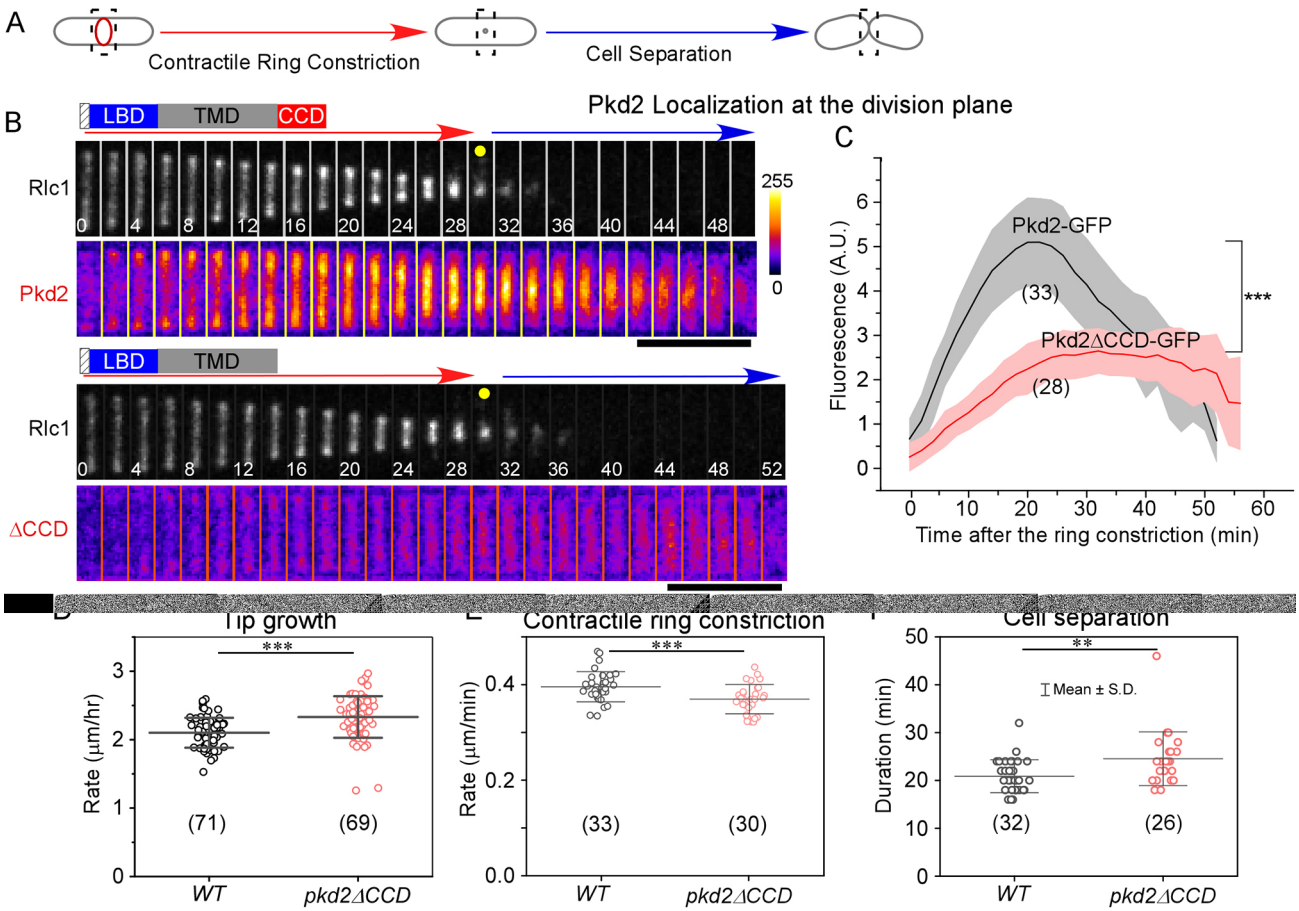

Fig. 4. Pkd2ΔCCD remains largely functional during both cell growth and cytokinesis. (A–C) Localization of Pkd2–GFP and Pkd2ΔCCD–GFP at the equatorial plane during cytokinesis. (A) Schematics of fission yeast cytokinesis. The actomyosin contractile ring is indicated in red. Dashed boxes indicate the equatorial division plane examined in B. (B) Time-series showing the division plane of a cell co-expressing the contractile ring marker Rlc1–tdTomato (gray) and either Pkd2–GFP or Pkd2ΔCCD–GFP (pseudo-colored). Numbers indicate the time in minutes after the start of contractile ring constriction. Yellow dots indicate completion of the ring constriction. The color bar indicates the fluorescence intensity scale. Red arrows represent the duration of the contractile ring constriction. Blue arrows represent the duration of the cell separation. Scale bar: 5 µm. (C) Time course of the fluorescence intensities of Pkd2–GFP and Pkd2ΔCCD–GFP in the division plane. The truncation mutant reduced the localization of Pkd2 at the equatorial plane by ∼50% (P<0.05). Solid lines show the mean, and shaded regions represent the s.d. (D) Tip growth rates of wild-type (*WT*) and *pkd2ΔCCD* mutant cells, measured by time-lapse microscopy at room temperature. (E,F) Progression of cytokinesis in *WT* and *pkd2ΔCCD* mutant cells. Dot plots of the contractile ring constriction rate (E) and the duration of cell separation (F) are shown. Bars represent mean±s.d. **P≤0.001; ***P≤0.0001 (two-tailed paired Student's *t*-test). All the data are pooled from at least two independent biological repeats. The numbers in C–F represent the numbers of cells analyzed.

fluorescence signal was present only in the ER (Fig. S4A). As for Pkd2, Trp663 and Trp1322 also possess an extracellular LBD, which shared the unique Ig-like fold consisting of eight β-strands (Fig. 5A). The transmembrane domains of both Trp663 and Trp1322 contain nine helices each. This was surprising as the secondary structure analysis using TMHMM (https://services.healthtech.dtu.dk/services/TMHMM-2.0) predicted eight and 11 helices for Trp663 and Trp1322, respectively. Lastly, both their cytoplasmic tails are disordered, like that of Pkd2 (Fig. 5A). Compared to Pkd2, Trp663 has the shortest CCD with 97 aa, whereas Trp1322 has the longest with 284 aa. We concluded that both Trp663 and Trp1322 are Pkd2 paralogues that possess a similar tripartite structure including an Ig-like LBD, a TMD with nine helices and a disordered CCD.

We then compared the intracellular localization of Pkd2 and its two paralogues. The localization of endogenous Trp663 and Trp1322 remained unknown, because both express too weakly to be detected (Morris et al., 2019). Therefore, we overexpressed both ectopically, tagged with either GFP (Fig. S4A) or mCherry (Fig. 5B,C) at the C-terminus, under the control of a strong actin promoter. As a control, we also ectopically overexpressed Pkd2. Although Pkd2–GFP continued to be targeted to the PM (Fig. S1A, middle), a larger fraction of Pkd2 was sorted to the endosomes and vacuoles compared to the endogenously expressed Pkd2 (Fig. S1A, middle). In comparison, Trp663 was targeted to the PM almost exclusively, largely absent from the intracellular membrane compartments (Fig. 5B; Fig. S4B). Compared with Pkd2 localization, Trp663 did not enrich at either the cell tips or the equatorial division plane (Fig. 5B, top). The depolarized distribution of Trp663 on the cell peripheries was similar to that of Pkd2ΔCCD–GFP (Fig. 5B, bottom). Unlike Pkd2 or Trp663 localization, Trp1322–mCherry was absent from the PM (Fig. 5C). Instead, Trp1322 localized to numerous intracellular puncta (Fig. 5C) where it often colocalized with Pkd2 (Fig. 5C). We concluded that these two Pkd2 paralogues occupy intracellular membrane compartments distinct from that of Pkd2.

Next, we compared the cellular functions of these two Pkd2 paralogues to Pkd2 through genetic studies. Expression of either Trp663 or Trp1322 failed to rescue the temperature-sensitive

Journal of Cell Science (2023) 136, jcs260598. doi:10.1242/jcs.260598

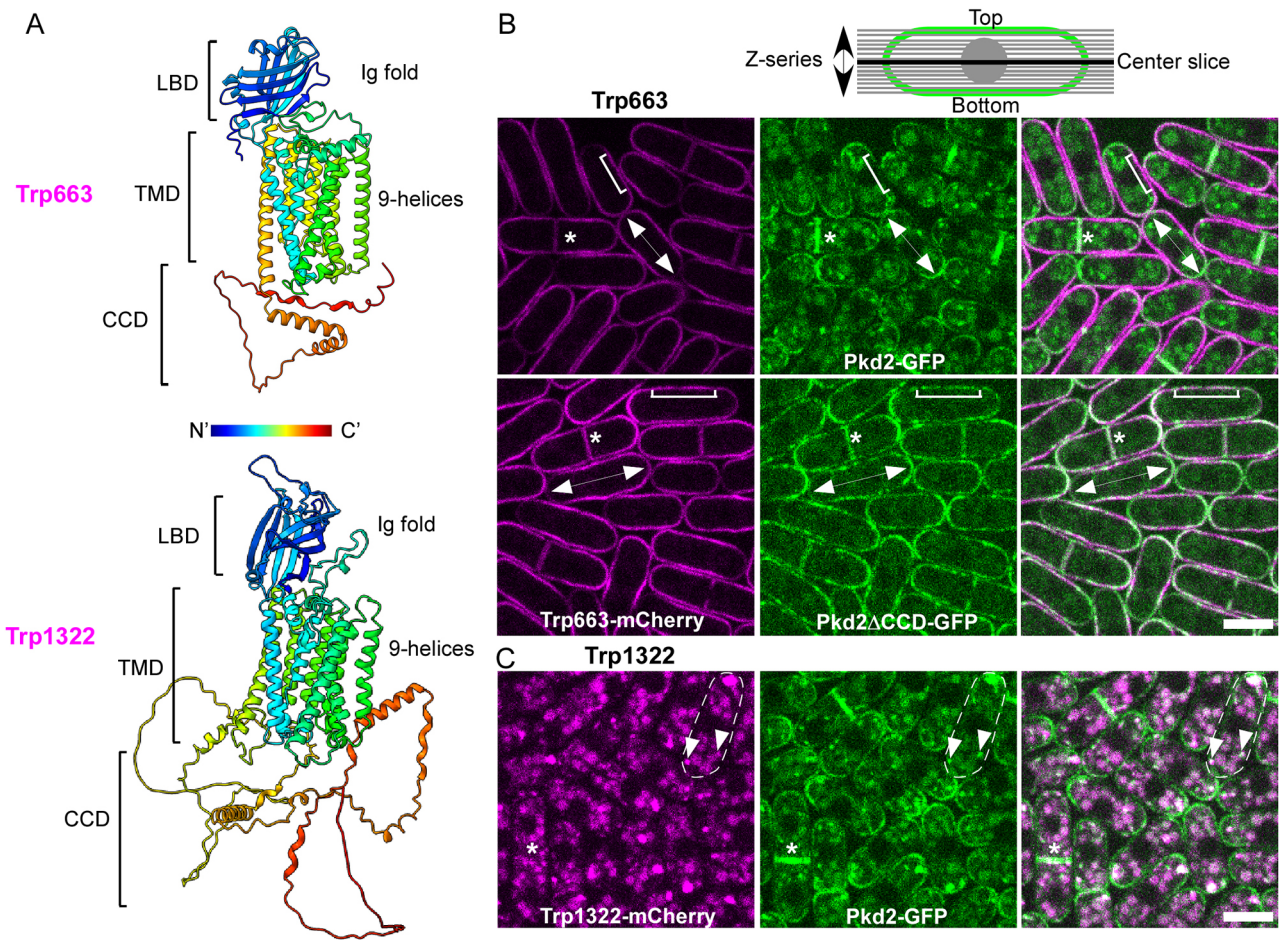

Fig. 5. Intracellular trafficking of Pkd2 differs from that of its two paralogues Trp663 and Trp1322. (A) Ribbon diagram of the AlphaFold predicted structures (rainbow colored) of Trp663 (top) and Trp1322 (bottom). Similar to Pkd2, their N-terminal SPs are projected to be cleaved before maturation. Therefore, they are not shown here. Both proteins possess an N-terminal LBD with a putative Ig-like fold, a nine-helix TMD and a largely disordered CCD. (B) Top: diagram of the center slice in the confocal *z*-series of a cell (side view). Bottom: micrographs (center slice) of cells co-expressing Trp663–mCherry (left, magenta) and either Pkd2–GFP or Pkd2ΔCCD–GFP (middle, green). Merged micrographs are shown on the right. Double-headed arrows indicate the cell tips. Brackets indicate the sides of the cells. Asterisks mark the equatorial division plane. Unlike Pkd2, Trp663 distributed evenly between the tip and the side of a cell. Scale bar: 5 µm. (C) Micrographs (center slice) of cells co-expressing Trp1322–mCherry (magenta) and Pkd2–GFP (green). Arrowheads indicate intracellular puncta where Trp1322 and Pkd2 colocalized in a representative cell (dashed outline). Images are representative of two independent experiments. Scale bar: 5 µm.

mutant *pkd2-B42*, unlike similarly expressed Pkd2 (Fig. S4B). Furthermore, neither *trp663Δ* nor *trp1322Δ* exhibited any negative genetic interactions with *pkd2-B42* (Fig. S4C). We concluded that the functions of these two Pkd2 paralogues do not overlap with those of Pkd2.

As the functions of Pkd2 and Trp663 do not overlap, we wondered whether this is due to their respective LBD or TMD domains. Firstly, we constructed a chimera between these two by replacing the LBD of Pkd2 with that of Trp663, $Trp663^{LBD}$–$Pkd2^{(TMD–CCD)}$ (hereafter chimera I) (Fig. 6A). This chimera, tagged with GFP, failed to reach the PM and remained in the ER (Fig. 6A). Although it rescued *pkd2-B42* (Fig. 6C and Table S2), it failed to revive the *pkd2Δ* mutant (Fig. 6D). Secondly, we replaced both the TMD and CCD of Pkd2 with those of Trp663 to construct another chimera, $Pkd2^{LBD}$–$Trp663^{(TMD–CCD)}$ (chimera II). This chimeric protein was only partially targeted to the PM. A portion of it remained in the ER (Fig. 6B). Chimera II failed to rescue *pkd2-B42* (Fig. 6C). Therefore, the TMD is not conserved between Pkd2 and Trp663, whereas the LBD is partially conserved between these two paralogues.

The localization and function of Pkd2 are conserved among fission yeast species

To determine whether the structure and function of Pkd2 are conserved in evolution, we first compared it to human polycystins. The most conserved regions between yeast Pkd2 and human PC-2 are the last two transmembrane helices of the TMD. The sequence of Pkd2 showed ∼20% identity with those of the human polycystins PC-1 and PC-2, and ∼22% sequence similarity with human PC-2 (Fig. S6). First, we expressed the presumed Pkd2 homologue human PC-2, tagged with GFP at its C-terminus, in fission yeast cells. Unlike Pkd2, PC-2–GFP stayed in the ER (Fig. S5A). Not surprisingly, it failed to rescue the *pkd2Δ* mutant (Fig. S5B), likely owing to the inability of PC-2 being targeted to the PM. As the LBD of Pkd2 is essential for its intracellular trafficking, we next made two chimeras, $Pkd2^{LBD}$–$PC1^{TMD}$ (chimera III) and $Pkd2^{(LBD+TM1)}$–$PC2^{TMD}$ (chimera IV), by appending the LBD to the TMDs of both human polycystins (Fig. S5C,D). Each was tagged with a fluorescence protein at its C-terminus and expressed from an exogenous locus. However, both chimeras remained in the ER, absent from the PM (Fig. S5D). As PC-1 and PC-2 can form

Journal of Cell Science (2023) 136, jcs260598. doi:10.1242/jcs.260598

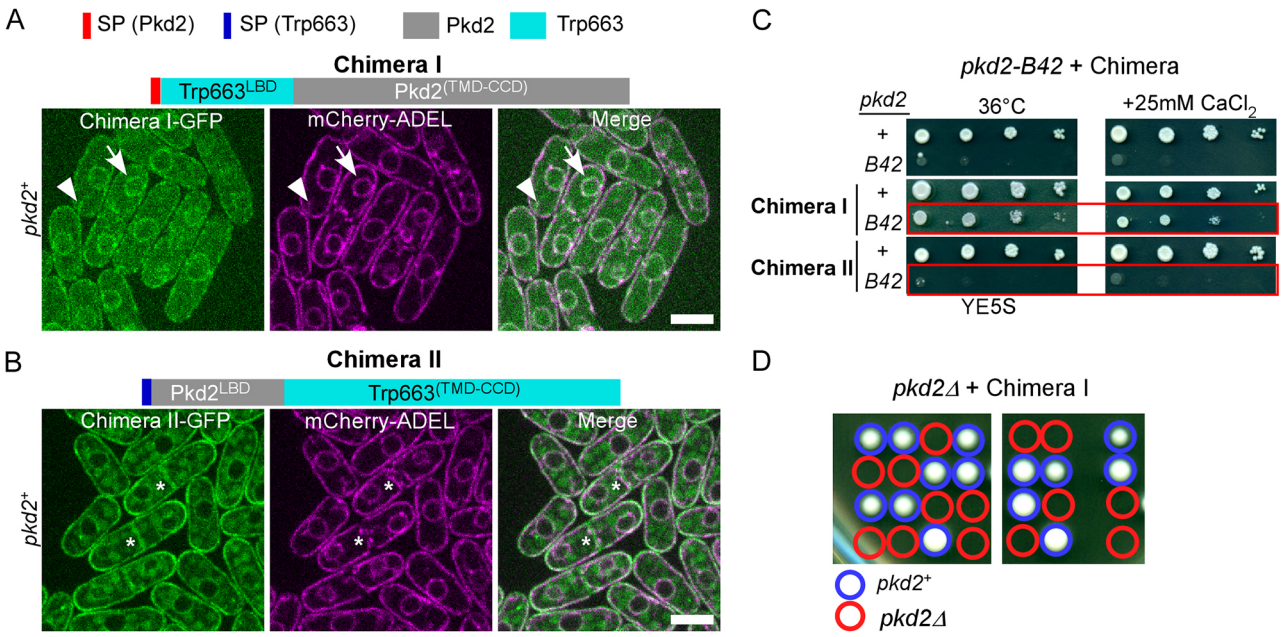

Fig. 6. A chimera of Pkd2 and Trp663 is partially functional. (A) Top: schematic of Chimera I in which the LBD of Pkd2 was replaced with that of Trp663. Bottom: micrographs (center slice) of cells expressing both chimera I tagged with GFP (green) and the ER marker mCherry–ADEL (magenta). Arrowheads indicate the ER tether and arrows indicate the peri-nuclear ER. Scale bar: 5 µm. (B) Top: schematic of chimera II in which the SP, TMD and CCD of Pkd2 were replaced with those of Trp663. Bottom: micrographs (center slice) of the cells expressing both chimera II tagged with GFP (green) and mCherry–ADEL (magenta). Asterisks indicate the equatorial division plane. Scale bar: 5 µm. (C) Ten-fold dilution series of yeast on either YE5S at 36°C (left) or YE5S plus 25 mM $CaCl_2$ (right) plates. (D) Representative tetrad dissection plates of the sporulated diploid *pkd2*$^+$/*pkd2Δ* expressing Chimera I–GFP. At least 20 tetrads were dissected with similar results. Images are representative of at least two independent experiments.

hetero-tetramers, we also co-expressed chimeras III and IV. Nevertheless, they continued to stay in the ER (Fig. S5E). Not surprisingly, these chimeras, whether expressed on their own or together, failed to rescue the temperature-sensitive mutant *pkd2-B42* (Fig. S5F). We concluded that fission yeast Pkd2 cannot be replaced by the human polycystins, most likely because of their failure to be trafficked to the PM.

Next, we determined whether Pkd2 has been conserved in the other fission yeast species. Besides *S. pombe*, there are three other fission yeast: *Schizosaccharomyces octosporus* (*So*), *Schizosaccharomyces cryophilus* (*Sc*) and *Schizosaccharomyces japonicus* (*Sj*) (Rhind et al., 2011). Through a BLAST search, we identified a single Pkd2 homologue in each of them. They share 63%, 62% and 49% sequence identity with Pkd2, respectively. For functional comparison, we chose *Sj*Pkd2 from *S. japonicus*, which is the most distant relative of *S. pombe* (Rhind et al., 2011). The putative topology of *Sj*Pkd2 was identical to that of Pkd2, as was its AlphaFold-predicted tripartite structure consisting of the LBD, TMD and CCD (Fig. 7A). When ectopically expressed in *S. pombe* cells, *Sj*Pkd2, tagged with GFP at its C-terminus, fully rescued the growth of *pkd2Δ* (Fig. 7B). *Sj*Pkd2–GFP was targeted effectively to the PM, concentrating at the cell tips during the growth and at the equatorial division plane during cytokinesis, as Pkd2 does (Fig. 7C). *Sj*Pkd2 was also visible in intracellular puncta, presumably representing the endosomes. To test whether the structures of these two Pkd2 homologues are conserved, we constructed a chimera (chimera V), by replacing LBD of Pkd2 with that of *Sj*Pkd2 (Fig. 7D). When ectopically expressed in *S. pombe* cells, this chimera rescued the growth of *pkd2Δ* partially, with slightly reduced efficiency compared to that of Pkd2 (Fig. 7B). The intracellular localization of chimera V was similar to that of *Sj*Pkd2, but a portion of the chimera stayed in the ER (Fig. 7D). We concluded that both the intracellular trafficking and function of Pkd2 are highly conserved in the clade of fission yeast species.

Based on our results, we proposed a novel model of the intracellular trafficking of Pkd2 throughout cell cycle (Fig. 8). This model explains the essential function of LBD and TMD in directing this mechanosensitive channel from the ER to the PM (Fig. 8, top). It also incorporates the critical role of CCD in both promoting the internalization of Pkd2 from the PM and preventing the clustering of the channel in eisosomes (Fig. 8, bottom).

DISCUSSION

Despite what we have learned about the cellular functions and localization of fission yeast polycystin Pkd2, little is known about its structure. Unlike human polycystins, the structure of Pkd2 has not been experimentally determined. Solving the structure of this transmembrane protein remains challenging, more so owing to the likely oligomerization of Pkd2. Like most TRP channels, human polycystins assemble into a tetramer, either as a homo- or hetero-tetramer (Grieben et al., 2017; Shen et al., 2016; Su et al., 2018; Wilkes et al., 2017). With such a constraint in mind, the AlphaFold prediction, despite its imperfection, provided us with the best available option to understand how the three domains of Pkd2 contribute to its function and intracellular trafficking. Through structure–function analysis, our study demonstrated for the first time that the intracellular trafficking of yeast Pkd2 plays a key role in activating and desensitizing this membrane tension-sensitive ion channel. Our finding sheds new light on the regulation of the mechanosensitive ion channels in general.

The predicted structure of LBD is unique in its Ig-like fold with a potential for lipid binding. To our knowledge, the arrangement of the eight β-strands of LBD is unlike that of any other Ig-like domain found so far (Bork et al., 1994). Although there is no direct

Journal of Cell Science (2023) 136, jcs260598. doi:10.1242/jcs.260598

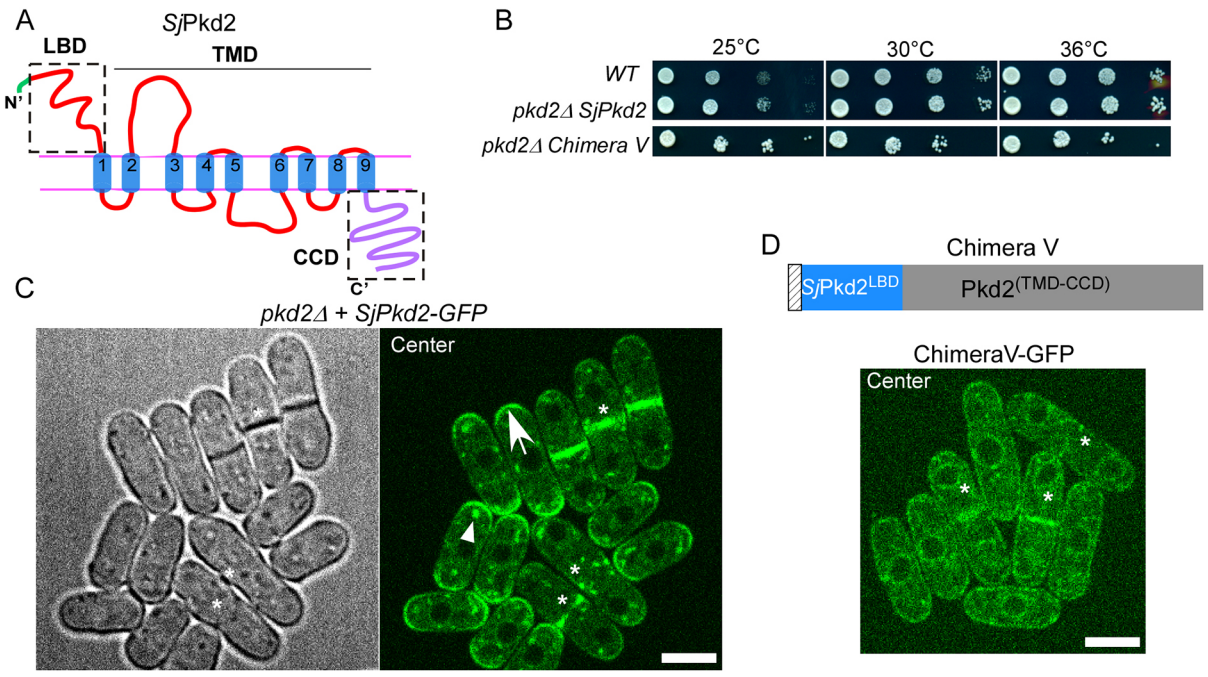

Fig. 7. The structure, function and intracellular trafficking of Pkd2 are conserved in the fission yeast *S. japonicus*. (A) Diagram of the predicted topology of *Sj*Pkd2 by Protter (Omasits et al., 2014). Green: N-terminal SP. (B) Ten-fold dilution series of *S. pombe* cells grown on YE5S plates at various temperatures. (C) Micrographs (center slice) of the *S. pombe pkd2Δ* mutant cells expressing *Sj*Pkd2–GFP. The arrow indicates the cell tip, asterisks mark cells in various stages of cytokinesis, and the arrowhead indicates intracellular puncta. Scale bar: 5 µm. (D) A chimera of Pkd2 and *Sj*Pkd2 can replace Pkd2 in *S. pombe*. Top: a diagram of Chimera V in which the LBD of Pkd2 was replaced with that of *Sj*Pkd2. Bottom: micrographs (center slice) of the *S. pombe* cells expressing Chimera V tagged with GFP. Asterisks indicate cells in various stages of cytokinesis. Unlike *Sj*Pkd2 or Pkd2, this chimera was only partially targeted to the PM. A portion of it stayed in the ER. Scale bar: 5 µm. Images are representative of at least two independent experiments.

biochemical evidence, sequence analysis suggested that LBD is an MD-2-related lipid-recognition (ML)-like domain found in both Der f 2, a major mite allergen (Ichikawa et al., 1998) and Niemann–Pick disease type C2 (NPC2) protein (Friedland et al., 2003). Both Der f 2 and NPC2 are capable of binding lipids directly (Johannessen et al., 2005). It is possible that LBD binds lipids such as ergosterol directly in the PM. However, LBD is surprisingly projected to be extracellular, in contrast to most other lipid-binding domains, which are imbedded in the membrane.

The LBD is essential for the trafficking of Pkd2 from the ER to the PM, where this mechanosensitive channel likely carries out its function as an influx channel. Without the LBD, Pkd2 is stuck in the ER. Although we cannot rule out the possibility that a portion of Pkd2 is functional at the ER, our data are most consistent with the model that Pkd2 is targeted to the PM where it can be activated. This is unlike the human polycystin PC-2, which is sorted to both the ER and PM. Nevertheless, future biochemical tests will be needed to determine the precise distribution of Pkd2 between the ER and PM. Because of the close contact between the LBD and TMD in the predicted structure, the LBD is likely also essential for the proper folding of Pkd2. The truncated mutant might remain in the ER as a misfolded protein. Although similar LBD domains are present in two fission yeast Pkd2 paralogues, Trp663 and Trp2322, neither can replace that of Pkd2 fully. Only the LBD of the Pkd2 ortholog in another fission yeast, *S. japonicus*, can. We predict that the LBD is highly conserved in other fungal Pkd2 orthologues as well.

In addition to its function in trafficking, LBD might also gate the ion channel pore of the Pkd2 channel, like the conserved TOP domain of human polycystins (Shen et al., 2016). Future studies will determine whether LBD can bind lipids directly *in vitro* and which lipids it binds.

In comparison to the LBD, the TMD is absolutely essential for the function of this mechanosensitive channel. This is most vividly displayed by the inability of the Pkd2–Trp663 chimera to rescue the *pkd2* deletion mutation. The chimera $Pkd2^{LBD}$–$Trp663^{(TMD–CCD)}$ reaches the PM. Nevertheless, it fails to replace the function of the wild-type Pkd2, despite the similar nine-helix fold of the TMD of Trp663. Future structural study of Pkd2 channel would be needed to determine the essential residues of the TMD. Mutating these key residues in each of the nine transmembrane helices would help us determine which one(s) of these helices is indispensable for the ion channel activity of Pkd2.

Unlike either the LBD or TMD, the CCD plays a critical role in regulating the internalization of Pkd2 and its distribution in the PM. Its role explains the polarized distribution of Pkd2, concentrating at the cell growth zones, unlike Trp663. This mostly disordered domain likely recruits adaptor proteins to internalize Pkd2 through endocytosis before being sent to vacuoles, the yeast equivalent of lysosomes. Such internalizations likely ‘desensitize’ Pkd2 to the membrane tension on the non-growth zone of fission yeast cells. This process mimics that of many GPCRs. Overall, Pkd2 achieves its enrichment at the cell tips and the equatorial division plane most likely through selective internalization.

Without the CCD, Pkd2 forms filament-like clusters on the PM, regulated by both eisosomes and ER–PM contacts. Although it has not been reported for Pkd2, such clustering on the PM is common among ion channels in animal cells (Sato et al., 2019). To our knowledge, this is the first documented example of clustering of an ion channel in yeast. Even more surprising is that the clustering is largely concentrated in eisosomes. Eisosomes or MCCs (membrane compartment of Can1) are furrowing microdomains of the yeast PM (Malinska et al., 2003; Young et al., 2002). Although Pkd2 is so far

Journal of Cell Science (2023) 136, jcs260598. doi:10.1242/jcs.260598

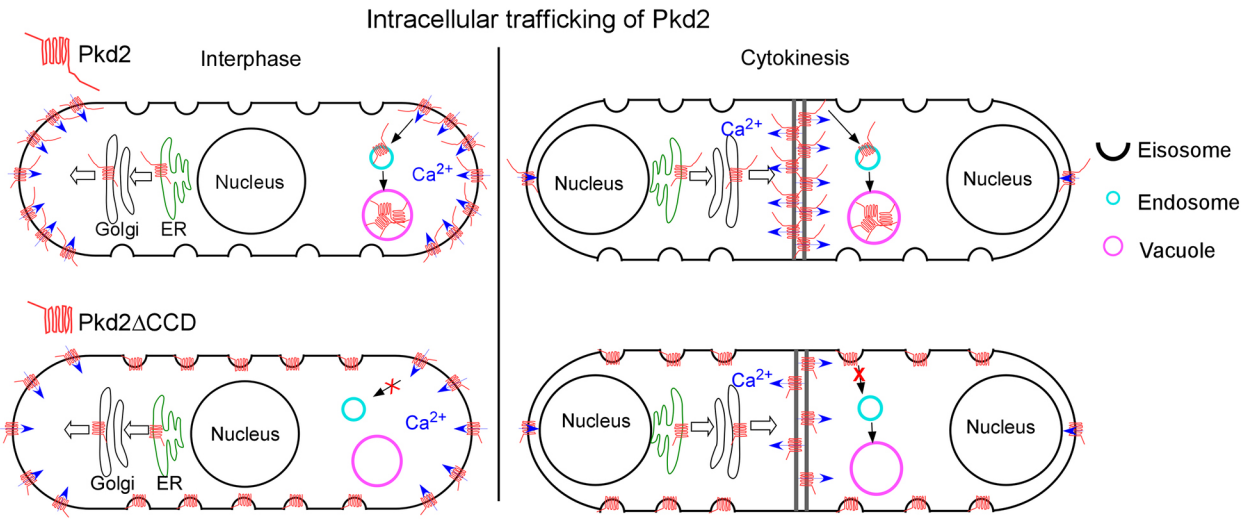

Fig. 8. A model of the intracellular trafficking of Pkd2. Top: intracellular trafficking of the full-length Pkd2. The transmembrane protein is synthesized in the ER where the N-terminal SP is cleaved. Pkd2 is then trafficked through the Golgi apparatus before being secreted to the PM, which depends on the N-terminal LBD. Upon reaching the PM, Pkd2 mostly resides in the growth zone of either cell tips during interphase (left) or division plane during cytokinesis (right). Outsides the growth zone, Pkd2 is selectively internalized through endocytosis and degraded in vacuoles, a process dependent on CCD. As a result of this intracellular trafficking route, the mechanosensitive Pkd2 channel distributes in a polarized pattern on the cell surface. When activated by the membrane stretching, Pkd2 directs the Ca^{2+} influx at the cell tip and equatorial division plane. Bottom: without the cytoplasmic tail, Pkd2ΔCCD fails to be internalized. Instead, it clusters in eisosomes in the PM on the sides of cells both during interphase (left) and cytokinesis (right). In these low-tension membrane compartments, the mechanosensitive Pkd2 channel is likely desensitized. As a result of clustering in eisosomes, the number of Pkd2ΔCCD molecules at either the tips or the division plane decreases significantly compared to the number for the full-length protein.

the only ion channel found in fission yeast eisosomes, many amino acid-polyamine-organocation (APC) transporters have been found there (Bianchi et al., 2018; Gournas et al., 2018; Moharir et al., 2018). The clustering of Pkd2 strongly suggests that it oligomerizes on the cell surface, like the human polycystins and many other ion channels. The clustering of Pkd2 in eisosomes is likely determined by the LBD, as eisosomes are rich in ergosterol (Grossmann et al., 2007).

Clustering of Pkd2 in eisosomes might keep this mechanosensitive channel from being hyper-active. Two likely roles of eisosomes have emerged (Appadurai et al., 2020). Firstly, they could prevent those APC transporters from being endocytosed and degraded (Grossmann et al., 2008). This might contribute to the reduced internalization of Pkd2 in the *pkd2ΔCCD* mutant. Secondly, this raft-like microdomain could provide the membrane reservoir when the cells need to expand their PM under mechanical stress (Kabeche et al., 2015; Lemière et al., 2021). Thus, the storage in eisosomes might serve as a mechanism to prevent Pkd2 from being hyper-activated as an ion channel. Surprisingly, disruption of ER–PM contacts, another microdomain of the PM, exacerbated clustering of Pkd2. These contact sites are well established as sites of lipid transfer between ER and the PM (Manford et al., 2012). One likely explanation for our observation is the increased lipid concentration in the PM of the membrane contact site mutant. Overall, the lipid composition of the PM can have a critical role in the intracellular trafficking of Pkd2.

In summary, we combined the predicted tertiary structure of the essential fission yeast channel Pkd2 with genetic analyses and quantitative microscopy to dissect its domains for the first time. The putative structure is likely conserved in both fission yeast and other fungi in which Pkd2 is a highly conserved essential protein (Hsiang and Baillie, 2005). Our study reveals the potential mechanism for trafficking this membrane tension-activated channel to the cell growth zone. It requires both ER-to-PM trafficking mediated by the LBD and targeted internalization depending on CCD. Our finding of the clustering of this putative ion channel in eisosomes indicates a novel role of this PM microdomain as a storage site for the membrane tension-sensing channels.

MATERIALS AND METHODS

Structure prediction

We used ChimeraX (UCSF) (Pettersen et al., 2004) to retrieve the predicted tertiary structure of a protein from AlphaFold based on its UniProt identifier. The Uniprot numbers for Pkd2, Trp663, Trp1322 and *Sj*Pkd2 are Q09917, O74520, O94543 and B6K7F8, respectively. All the structures in the figures were also rendered using ChimeraX.

Yeast genetics and cell culture

We followed the standard protocols for yeast cell culture and genetics (Moreno et al., 1991). Fission yeast tetrads were sporulated on sporulation agar with five supplements (SPA5S) plates and dissected using a SporePlay+ dissection microscope (Singer Instruments, UK). Transformation of yeast used the standard lithium-acetate method. All the strains used in this study are listed in Table S3.

For assays of viability, overnight cultures were diluted and grown for an additional 6 h before being spotted for the ten-fold dilution series. To measure growth curves in liquid culture, we diluted overnight cultures to an optical density of 0.3 at A_{600nm}. We then measured the cell density with a spectrometer (Eppendorf) every 2 h for the next 10 h, followed by the final measurement at 24 h.

Cloning and expression of Pkd2 truncation mutants, chimeras and other TRP channels

For molecular cloning, both the gene of interest and the vector were amplified by PCR using Q5 polymerase (New England Biolabs, USA). Unless specified, most of the vectors used were either pAV0714 (for tagging a construct with GFP) or pAV0328 (for tagging a construct with mCherry) (Vještica et al., 2020). After being digested with DpnI, the PCR products were purified using NucleoSpin Gel and PCR Clean-up kit (Macherey-Nagel, 740609). Purified PCR products were assembled together using NEBuilder HiFi DNA assembly kit (New England Biolabs, E2621). After being verified by Sanger sequencing, 2 µg plasmid was linearized with the restriction enzyme AfeI and integrated into the *ura4* locus in the yeast

genome. For the constructs that were integrated at the *ade6* locus, a new vector was generated by replacing the GFP sequence in the vector pAV0661 (Vještica et al., 2020) with that of mCherry, and the resulting vector was linearized by PmeI. The linearized vectors were purified and then transformed into yeast using the lithium-acetate method. mEGFP was used to tag the Pkd2 truncation mutants at their endogenous locus or from the *leu1* locus. Super-fold GFP (sfGFP) was used for constructs expressed from the *ura4* locus.

The LBD–GFP was expressed at the *leu1* locus driven by the *3nmt1* promoter. To construct the LBD–GFP expression vector, the DNA sequence of LBD including that of the SP was amplified and cloned into the vector pFA-kanMX6-3nmt1GFP (lab stock, Bähler et al., 1998) using the HiFi assembly kit. The DNA fragment encoding P3nmt1-LBD-GFP was then integrated into the *leu1* locus through PCR-based homologous recombination (Bähler et al., 1998). For N-terminal GFP tagging of Pkd2 and Trp663, either 3nmt1-GFP or 41nmt1-GFP was integrated at the N-terminus of the respective gene at the endogenous locus using PCR-based gene targeting (Bähler et al., 1998).

Microscopy

For microscopy, 1–2 ml of exponentially growing yeast cells at 25°C with a density between 5.0×10^6/ml and 1.0×10^7/ml in yeast extract with five supplements (YE5S) liquid medium (unless specified) were harvested by centrifugation at 1500 ***g*** for 1 min and resuspended in 50 µl YE5S. Resuspended cells (6 µl) were spotted to a 25% gelatin with a YE5s pad and sealed under the coverslip using VALAP (1:1:1 mixture of Vaseline, lanolin and paraffin) (Wang et al., 2016).

Live-cell microscopy was carried out on an Olympus IX71 microscope. It was equipped with 100× (NA=1.40) and 60× (NA=1.40) objective lenses, a confocal spinning-disk unit (CSU-X1; Yokogawa, Japan), a motorized *xy* stage with a Piezo Z Top plate (Applied Scientific Instrumentation). The microscope is housed in a designated microscopy room where the temperature is maintained at around 22±2°C. The images were captured on an Ixon-897 EMCCD camera controlled by iQ3.0 (Andor, Ireland). Solid-state lasers of 488 and 561 nm were used for imaging green and red fluorescence, respectively. For time-lapse microscopy, the cells were imaged for 2 h with 2-min intervals and with *Z*-series of 15 slices at a step size of 0.5 µm. To help minimize the potential variations in culture and microscopy conditions, the wild-type control and the experimental groups were imaged on the same day. Bright-field microscopy was used for the quantification of deflated cells.

For calcofluor staining, 2 ml of exponentially growing cells were harvested at 1500 ***g*** for 1 min. The cells were fixed in 4% paraformaldehyde while being rotated for 10 mins. We spun down the fixed cells and washed them three times with 1 ml of TEMK buffer (50 mM Tris-HCl pH 7.4, 1 mM $MgCl_2$, 50 mM KCl, 1 mM EGTA). The washed cells were re-suspended in 1 ml TEMK buffer and stored at 4°C until the next day. Just before imaging, 1 µl of calcofluor solution (1 µg/ml) (Sigma-Aldrich, 18909) was added to 1 ml of cells. The cells were stained while being rotated on a rocker in the dark for 5 min before they were pelleted and resuspended in 50 µl TEMK. The stained sample (5 µl) was spotted directly on a glass slide, covered with a coverslip, and sealed with VALAP. Images were taken with a 60× objective lens using an epifluorescence microscope (Olympus IX81) equipped with a mercury lamp and a digital camera.

Image processing and analysis

ImageJ (National Institutes of Health) was used for processing all the images with either freely available or customized macros/plug-ins. For quantitative analysis of the fluorescence micrographs of a time-lapse series, we first corrected *x*-*y* drifting using StackReg (Thevenaz et al., 1998). Average intensity projections of *z*-slices were used for quantification. Kymographs of the time-series of the contractile rings were generated to determine both the start and end of ring closure.

To quantify the colocalization between two proteins, maximum-intensity projections of the two top slices of a full *z*-series in which the green fluorescence was visible were generated. The ImageJ (Fiji) macro Coloc2 was used to quantify the Pearson's correlation coefficient (R) (no threshold). R-value <0.1 was considered as no colocalization, 0.1–0.5 as partial colocalization and >0.5 as significant colocalization.

Acknowledgements

We would like to thank Dr Zhang Dan (Temasek Life Sciences Laboratory, Singapore), Dr Snezhana Oliferenko (King's College, London, UK) and Dr James Moseley (Geisel School of Medicine, Dartmouth, NH, USA) for sharing their yeast strains, and Dr Sophie Martin (University of Lausanne, Switzerland) for sharing the pAV0714 plasmid. We thank Dr Steven Chou (University of Connecticut) for assisting with our structure prediction using AlphaFold. We acknowledge the National BioResource Project (NBRP)-Yeast (Japan) for sending the yeast strains. We also thank the Chen lab members Abhishek Poddar and Clare Muller at the University of Toledo for technical assistance.

Competing interests

The authors declare no competing or financial interests.

Author contributions

Conceptualization: Q.C.; Methodology: M.M., D.S., Q.C.; Software: Q.C.; Validation: M.M., D.S., P.C.; Formal analysis: M.M., D.S., Q.C.; Investigation: M.M., D.S., P.C., B.T.B., Q.C.; Data curation: M.M., D.S., Q.C.; Writing - original draft: M.M., Q.C.; Writing - review & editing: M.M., Q.C.; Visualization: M.M., D.S., Q.C.; Supervision: Q.C.; Funding acquisition: Q.C.

Funding

This work was supported by the National Institutes of Health grants R15GM134496 and R01GM144652 to Q.C., and the National Science Foundation grant 2144701 to Q.C. The content is solely the responsibility of the authors and does not necessarily represent the official views of the National Institutes of Health. The authors declare no conflicts of interests. Deposited in PMC for release after 12 months.

Data availability

All relevant data can be found within the article and its supplementary information.

Peer review history

The peer review history is available online at https://journals.biologists.com/jcs/lookup/doi/10.1242/jcs.260598.reviewer-comments.pdf

References

Appadurai, D., Gay, L., Moharir, A., Lang, M. J., Duncan, M. C., Schmidt, O., Teis, D., Vu, T. N., Silva, M., Jorgensen, E. M. et al. (2020). Plasma membrane tension regulates eisosome structure and function. *Mol. Biol. Cell* **31**, 287-303. doi:10.1091/mbc.E19-04-0218

Bähler, J., Wu, J. Q., Longtine, M. S., Shah, N. G., Mckenzie, A., III, Steever, A. B., Wach, A., Philippsen, P., Pringle, J. R. and Pringle, J. R. (1998). Heterologous modules for efficient and versatile PCR–based gene targeting in Schizosaccharomyces pombe. *Yeast* **14**, 943-951. doi:10.1002/(SICI)1097-0061(199807)14:10<943::AID-YEA292>3.0.CO;2-Y

Bianchi, F., Syga, L., Moiset, G., Spakman, D., Schavemaker, P. E., Punter, C. M., Seinen, A. B., Van Oijen, A. M., Robinson, A. and Poolman, B. (2018). Steric exclusion and protein conformation determine the localization of plasma membrane transporters. *Nat. Commun.* **9**, 501. doi:10.1038/s41467-018-02864-2

Bork, P., Holm, L. and Sander, C. (1994). The immunoglobulin fold. Structural classification, sequence patterns and common core. *J. Mol. Biol.* **242**, 309-320. doi:10.1006/jmbi.1994.1582

Burn, T. C., Connors, T. D., Dackowski, W. R., Petry, L. R., Van Raay, T. J., Millholland, J. M., Venet, M., Miller, G., Hakim, R. M., Landes, G. M. et al. (1995). Analysis of the genomic sequence for the autosomal dominant polycystic kidney disease (PKD1) gene predicts the presence of a leucine-rich repeat. The American PKD1 Consortium (APKD1 Consortium). *Hum. Mol. Genet.* **4**, 575-582. doi:10.1093/hmg/4.4.575

Cai, Y., Maeda, Y., Cedzich, A., Torres, V. E., Wu, G., Hayashi, T., Mochizuki, T., Park, J. H., Witzgall, R. and Somlo, S. (1999). Identification and characterization of polycystin-2, the PKD2 gene product. *J. Biol. Chem.* **274**, 28557-28565. doi:10.1074/jbc.274.40.28557

Foggensteiner, L., Bevan, A. P., Thomas, R., Coleman, N., Boulter, C., Bradley, J., Ibraghimov-Beskrovnaya, O., Klinger, K. and Sandford, R. (2000). Cellular and subcellular distribution of polycystin-2, the protein product of the PKD2 gene. *J. Am. Soc. Nephrol.* **11**, 814-827. doi:10.1681/ASN.V115814

Friedland, N., Liou, H.-L., Lobel, P. and Stock, A. M. (2003). Structure of a cholesterol-binding protein deficient in Niemann–Pick type C2 disease. *Proc. Natl. Acad. Sci. USA* **100**, 2512-2517. doi:10.1073/pnas.0437840100

Geng, L., Segal, Y., Peissel, B., Deng, N., Pei, Y., Carone, F., Rennke, H. G., Glücksmann-Kuis, A. M., Schneider, M. C. and Ericsson, M. et al. (1996). Identification and localization of polycystin, the PKD1 gene product. *J. Clin. Invest.* **98**, 2674-2682. doi:10.1172/JCI119090

Gournas, C., Gkionis, S., Carquin, M., Twyffels, L., Tyteca, D. and Andre, B. (2018). Conformation-dependent partitioning of yeast nutrient transporters into starvation-protective membrane domains. *Proc. Natl. Acad. Sci. U.S.A.* **115**, E3145-E3154. doi:10.1073/pnas.1719462115

Grieben, M., Pike, A. C., Shintre, C. A., Venturi, E., El-Ajouz, S., Tessitore, A., Shrestha, L., Mukhopadhyay, S., Mahajan, P., Chalk, R. et al. (2017). Structure of the polycystic kidney disease TRP channel Polycystin-2 (PC2). *Nat. Struct. Mol. Biol.* **24**, 114-122. doi:10.1038/nsmb.3343

Grossmann, G., Opekarova, M., Malinsky, J., Weig-Meckl, I. and Tanner, W. (2007). Membrane potential governs lateral segregation of plasma membrane proteins and lipids in yeast. *EMBO J.* **26**, 1-8. doi:10.1038/sj.emboj.7601466

Grossmann, G., Malinsky, J., Stahlschmidt, W., Loibl, M., Weig-Meckl, I., Frommer, W. B., Opekarova, M. and Tanner, W. (2008). Plasma membrane microdomains regulate turnover of transport proteins in yeast. *J. Cell Biol.* **183**, 1075-1088. doi:10.1083/jcb.200806035

Hogan, M. C., Manganelli, L., Woollard, J. R., Masyuk, A. I., Masyuk, T. V., Tammachote, R., Huang, B. Q., Leontovich, A. A., Beito, T. G., Madden, B. J. et al. (2009). Characterization of PKD protein-positive exosome-like vesicles. *J. Am. Soc. Nephrol.* **20**, 278-288. doi:10.1681/ASN.2008060564

Hoya, M., Yanguas, F., Moro, S., Prescianotto-Baschong, C., Doncel, C., De Leon, N., Curto, M. A., Spang, A. and Valdivieso, M. H. (2017). Traffic through the trans-Golgi network and the endosomal system requires collaboration between exomer and clathrin adaptors in fission yeast. *Genetics* **205**, 673-690. doi:10.1534/genetics.116.193458

Hsiang, T. and Baillie, D. L. (2005). Comparison of the yeast proteome to other fungal genomes to find core fungal genes. *J. Mol. Evol.* **60**, 475-483. doi:10.1007/s00239-004-0218-1

Ichikawa, S., Hatanaka, H., Yuuki, T., Iwamoto, N., Kojima, S., Nishiyama, C., Ogura, K., Okumura, Y. and Inagaki, F. (1998). Solution structure of Der f 2, the major mite allergen for atopic diseases. *J. Biol. Chem.* **273**, 356-360. doi:10.1074/jbc.273.1.356

Johannessen, B. R., Skov, L. K., Kastrup, J. S., Kristensen, O., Bolwig, C., Larsen, J. N., Spangfort, M., Lund, K. and Gajhede, M. (2005). Structure of the house dust mite allergen Der f 2: implications for function and molecular basis of IgE cross-reactivity. *FEBS Lett.* **579**, 1208-1212. doi:10.1016/j.febslet.2004.11.115

Jumper, J., Evans, R., Pritzel, A., Green, T., Figurnov, M., Ronneberger, O., Tunyasuvunakool, K., Bates, R., Žídek, A. and Potapenko, A. (2021). Highly accurate protein structure prediction with AlphaFold. *Nature* **596**, 583-589. doi:10.1038/s41586-021-03819-2

Kabeche, R., Baldissard, S., Hammond, J., Howard, L. and Moseley, J. B. (2011). The filament-forming protein Pil1 assembles linear eisosomes in fission yeast. *Mol. Biol. Cell* **22**, 4059-4067. doi:10.1091/mbc.e11-07-0605

Kabeche, R., Howard, L. and Moseley, J. B. (2015). Eisosomes provide membrane reservoirs for rapid expansion of the yeast plasma membrane. *J. Cell Sci.* **128**, 4057-4062. doi:10.1242/jcs.176867

Lemière, J., Ren, Y. and Berro, J. (2021). Rapid adaptation of endocytosis, exocytosis, and eisosomes after an acute increase in membrane tension in yeast cells. *Elife* **10**, e62084. doi:10.7554/eLife.62084

Liu, X., Vien, T., Duan, J., Sheu, S.-H., Decaen, P. G. and Clapham, D. E. (2018). Polycystin-2 is an essential ion channel subunit in the primary cilium of the renal collecting duct epithelium. *Elife* **7**, e33183. doi:10.7554/eLife.33183

Malinska, K., Malinsky, J., Opekarova, M. and Tanner, W. (2003). Visualization of protein compartmentation within the plasma membrane of living yeast cells. *Mol. Biol. Cell* **14**, 4427-4436. doi:10.1091/mbc.e03-04-0221

Manford, A. G., Stefan, C. J., Yuan, H. L., Macgurn, J. A. and Emr, S. D. (2012). ER-to-plasma membrane tethering proteins regulate cell signaling and ER morphology. *Dev. Cell* **23**, 1129-1140. doi:10.1016/j.devcel.2012.11.004

Marek, M., Vincenzetti, V. and Martin, S. G. (2020). Sterol biosensor reveals LAM-family Ltc1-dependent sterol flow to endosomes upon Arp2/3 inhibition. *J. Cell Biol.* **219**, e202001147. doi:10.1083/jcb.202001147

Mochizuki, T., Wu, G., Hayashi, T., Xenophontos, S. L., Veldhuisen, B., Saris, J. J., Reynolds, D. M., Cai, Y., Gabow, P. A., Pierides, A. et al. (1996). PKD2, a gene for polycystic kidney disease that encodes an integral membrane protein. *Science.* **272**, 1339-1342. doi:10.1126/science.272.5266.1339

Moharir, A., Gay, L., Appadurai, D., Keener, J. and Babst, M. (2018). Eisosomes are metabolically regulated storage compartments for APC-type nutrient transporters. *Mol. Biol. Cell* **29**, 2113-2127. doi:10.1091/mbc.E17-11-0691

Moreno, S., Klar, A. and Nurse, P. (1991). Molecular genetic analysis of fission yeast Schizosaccharomyces pombe. *Methods Enzymol.* **194**, 795-823. doi:10.1016/0076-6879(91)94059-L

Morris, Z., Sinha, D., Poddar, A., Morris,, B. and Chen, Q. (2019). Fission yeast TRP channel Pkd2p localizes to the cleavage furrow and regulates cell separation during cytokinesis. *Mol. Biol. Cell* **30**, 1791-1804. doi:10.1091/mbc.E18-04-0270

Mulholland, J., Konopka, J., Singer-Kruger, B., Zerial, M. and Botstein, D. (1999). Visualization of receptor-mediated endocytosis in yeast. *Mol. Biol. Cell* **10**, 799-817. doi:10.1091/mbc.10.3.799

Nauli, S. M., Alenghat, F. J., Luo, Y., Williams, E., Vassilev, P., Li, X., Elia, A. E., Lu, W., Brown, E. M., Quinn, S. J. et al. (2003). Polycystins 1 and 2 mediate mechanosensation in the primary cilium of kidney cells. *Nat. Genet.* **33**, 129-137. doi:10.1038/ng1076

Ng, A. Q. E., Ng, A. Y. E. and Zhang, D. (2020). Plasma membrane furrows control plasticity of ER-PM contacts. *Cell Reports* **30**, 1434-1446.e7. doi:10.1016/j.celrep.2019.12.098

Omasits, U., Ahrens, C. H., Muller, S. and Wollscheid, B. (2014). Protter: interactive protein feature visualization and integration with experimental proteomic data. *Bioinformatics* **30**, 884-886. doi:10.1093/bioinformatics/btt607

Palmer, C. P., Aydar, E. and Djamgoz, M. B. (2005). A microbial TRP-like polycystic-kidney-disease-related ion channel gene. *Biochem. J.* **387**, 211-219. doi:10.1042/BJ20041710

Parnell, S. C., Magenheimer, B. S., Maser, R. L., Pavlov, T. S., Havens, M. A., Hastings, M. L., Jackson, S. F., Ward, C. J., Peterson, K. R. and Staruschenko, A. (2018). A mutation affecting polycystin-1 mediated heterotrimeric G-protein signaling causes PKD. *Hum. Mol. Genet.* **27**, 3313-3324. doi:10.1093/hmg/ddy223

Pazour, G. J., San Agustin, J. T., Follit, J. A., Rosenbaum, J. L. and Witman, G. B. (2002). Polycystin-2 localizes to kidney cilia and the ciliary level is elevated in orpk mice with polycystic kidney disease. *Curr. Biol.* **12**, R378-R380. doi:10.1016/S0960-9822(02)00877-1

Pennekamp, P., Karcher, C., Fischer, A., Schweickert, A., Skryabin, B., Horst, J., Blum, M. and Dworniczak, B. (2002). The ion channel polycystin-2 is required for left-right axis determination in mice. *Curr. Biol.* **12**, 938-943. doi:10.1016/S0960-9822(02)00869-2

Pettersen, E. F., Goddard, T. D., Huang, C. C., Couch, G. S., Greenblatt, D. M., Meng, E. C. and Ferrin, T. E. (2004). UCSF Chimera - a visualization system for exploratory research and analysis. *J. Comput. Chem.* **25**, 1605-1612. doi:10.1002/jcc.20084

Poddar, A., Sidibe, O., Ray, A. and Chen, Q. (2021). Calcium spikes accompany cleavage furrow ingression and cell separation during fission yeast cytokinesis. *Mol. Biol. Cell* **32**, 15-27. doi:10.1091/mbc.E20-09-0609

Poddar, A., Hsu, Y. Y., Zhang, F., Shamma, A., Kreais, Z., Muller, C., Malla, M., Ray, A., Liu, A. and Chen, Q. (2022). Membrane stretching activates calcium-permeability of a putative channel Pkd2 during fission yeast cytokinesis. *Mol. Biol. Cell* **33**, ar134. doi:10.1091/mbc.E22-07-0248

Qian, F., Boletta, A., Bhunia, A. K., Xu, H., Liu, L., Ahrabi, A. K., Watnick, T. J., Zhou, F. and Germino, G. G. (2002). Cleavage of polycystin-1 requires the receptor for egg jelly domain and is disrupted by human autosomal-dominant polycystic kidney disease 1-associated mutations. *Proc. Natl. Acad. Sci. U.S.A.* **99**, 16981-16986. doi:10.1073/pnas.252484899

Rhind, N., Chen, Z., Yassour, M., Thompson, D. A., Haas, B. J., Habib, N., Wapinski, I., Roy, S., Lin, M. F., Heiman, D. I. et al. (2011). Comparative functional genomics of the fission yeasts. *Science* **332**, 930-936. doi:10.1126/science.1203357

Sato, D., Hernandez-Hernandez, G., Matsumoto, C., Tajada, S., Moreno, C. M., Dixon, R. E., O'dwyer, S., Navedo, M. F., Trimmer, J. S., Clancy, C. E. et al. (2019). A stochastic model of ion channel cluster formation in the plasma membrane. *J. Gen. Physiol.* **151**, 1116-1134. doi:10.1085/jgp.201912327

Shen, P. S., Yang, X., Decaen, P. G., Liu, X., Bulkley, D., Clapham, D. E. and Cao, E. (2016). The structure of the polycystic kidney disease channel PKD2 in lipid nanodiscs. *Cell* **167**, 763-773.e11. doi:10.1016/j.cell.2016.09.048

Sinha, D., Ivan, D., Gibbs, E., Chetluru, M., Goss, J. and Chen, Q. (2022). Fission yeast polycystin Pkd2p promotes cell size expansion and antagonizes the Hippo-related SIN pathway. *J. Cell Sci.* **135**, jcs259046. doi:10.1242/jcs.259046

Su, X., Wu, M., Yao, G., El-Jouni, W., Luo, C., Tabari, A. and Zhou, J. (2015). Regulation of polycystin-1 ciliary trafficking by motifs at its C-terminus and polycystin-2 but not by cleavage at the GPS site. *J. Cell Sci.* **128**, 4063-4073. doi:10.1242/jcs.160556

Su, Q., Hu, F., Ge, X., Lei, J., Yu, S., Wang, T., Zhou, Q., Mei, C. and Shi, Y. (2018). Structure of the human PKD1-PKD2 complex. *Science* **361**, eaat9819. doi:10.1126/science.aat9819

Teufel, F., Almagro Armenteros, J. J., Johansen, A. R., Gislason, M. H., Pihl, S. I., Tsirigos, K. D., Winther, O., Brunak, S., Von Heijne, G. and Nielsen, H. (2022). SignalP 6.0 predicts all five types of signal peptides using protein language models. *Nat. Biotechnol.* **40**, 1023-1025. doi:10.1038/s41587-021-01156-3

Thevenaz, P., Ruttimann, U. E. and Unser, M. (1998). A pyramid approach to subpixel registration based on intensity. *IEEE Trans. Image Process.* **7**, 27-41. doi:10.1109/83.650848

Vještica, A., Marek, M., Nkosi, P. J., Merlini, L., Liu, G., Bérard, M., Billault-Chaumartin, I. and Martin, S. G. (2020). A toolbox of stable integration vectors in the fission yeast Schizosaccharomyces pombe. *J. Cell Sci.* **133**, jcs240754. doi:10.1242/jcs.240754

Wang, J., Silva, M., Haas, L. A., Morsci, N. S., Nguyen, K. C., Hall, D. H. and Barr, M. M. (2014). C. elegans ciliated sensory neurons release extracellular vesicles that function in animal communication. *Curr. Biol.* **24**, 519-525. doi:10.1016/j.cub.2014.01.002

Wang, N., Lee, I.-J., Rask, G. and Wu, J.-Q. (2016). Roles of the TRAPP-II complex and the exocyst in membrane deposition during fission yeast cytokinesis. *PLoS Biol.* **14**, e1002437. doi:10.1371/journal.pbio.1002437

Wilkes, M., Madej, M. G., Kreuter, L., Rhinow, D., Heinz, V., De Sanctis, S., Ruppel, S., Richter, R. M., Joos, F., Grieben, M. et al. (2017). Molecular insights into lipid-assisted Ca2+ regulation of the TRP channel Polycystin-2. *Nat. Struct. Mol. Biol.* **24**, 123-130. doi:10.1038/nsmb.3357

Young, M. E., Karpova, T. S., Brugger, B., Moschenross, D. M., Wang, G. K., Schneiter, R., Wieland, F. T. and Cooper, J. A. (2002). The Sur7p family defines novel cortical domains in Saccharomyces cerevisiae, affects sphingolipid metabolism, and is involved in sporulation. *Mol. Cell. Biol.* **22**, 927-934. doi:10.1128/MCB.22.3.927-934.2002

Zhang, D., Vjestica, A. and Oliferenko, S. (2012). Plasma membrane tethering of the cortical ER necessitates its finely reticulated architecture. *Curr. Biol.* **22**, 2048-2052. doi:10.1016/j.cub.2012.08.047